ASPS Conference Proceedings 1: 1449-1453 (2022)

Proceedings of

12th Structural Engineering Convention-An International Event (SEC 2022)

Available at https://asps-journals.com/index.php/acp

# Failure mechanisms and curvature radius effect in fixed ended flat oval LDSS slender column under axial compression

Khwairakpam Sachidananda [1,*], Konjengbam Darunkumar Singh [2]

[1] Department of Civil Engineering, Assistant Professor, National Institute of Technology Manipur, Langol, Manipur, 795 004, India
[2] Department of Civil Engineering, Professor, Indian Institute of Technology Guwahati, Guwahati, Assam, 781 039, India

**Paper ID - 130422**

**Abstract**

This paper presents the different failure mechanism of fixed ended flat oval LDSS (Lean Duplex Stainless Steel) slender column under axial compression by using the finite element software Abaqus. The load capacity is presented in terms of yield load and the deformation modes at ultimate load ($\delta_u$) and post ultimate load at 1.5 $\delta_u$. Based on the deformation at ultimate deformation ($\delta_u$) and post ultimate load at 1.5$\delta_{u,}$ failure mechanisms are identified as viz., 1) Local to local yielded buckling, 2) Local to local yielded flexural, 3) Flexural to flexural yielding, which ultimately depend on the slenderness of the column. The low slenderness column was found to have higher load capacity of column as compared to the higher slenderness column. The parametric effect of changes of curvature radius of cross-section on ultimate strength of column has also been presented showing the semi-circle section to have the highest strength.

*Keywords*: Abaqus, flat oval, failure, mechanism, Curvature-radius.

## 1. Introduction

The cold formed stainless steel was the most popular steel for construction industry due to numerous advantages of aesthetic appearance, corrosion resistance, high strength, smooth and uniform surface etc. The construction industry shifted its construction of concrete structures to the light weight steel which gives benefit in terms of light weight, high speed construction, higher scrap values etc. Austenitic and ferritic are the most common types of stainless steel with nickel content of ~8%- 11%. Out of many components of stainless steel, nickel determined the price of stainless steel. The introduction of new type of stainless steel i.e. LDSS (Lean duplex stainless steel) with higher strength of around twice the strength of austenitic, ferrite and lower nickel content of ~1.5 give the most economic stainless steel (Theofanous and Gardner, 2010; EN 10088-4, Patton and Singh, 2012). The construction industry uses steels in different forms of closed and open sections like circle, square, I, rectangle, L, T, + etc. In comparison with open section, closed formed steel are having more advantages due to its higher moment of inertia giving higher strength. Many researchers are investigating sections like square (Liu and Young, 2003; Theofanous and Gardner, 2009), circular (Ellobody and Young, 2007), oval (Zhu and Young, 2011, 2012; Gardner and Ministro, 2004), L,T,+ (Patton and Singh, 2012, 2013), ellipse (Chan and gardner, 2008) etc. Among all these sections, flat oval section is one of the newest sections and much information is needed to know the strength of the section as various members like beam, column etc. The Column usually exist in various form of short and slender column based on the length of the column and its properties are different. The failures of the short column are usually termed as local buckling and the slender column as flexural column. But usually the failure mechanisms are different for different length of the column. In the present study, only the thin slender cross section under Class 4 EN 1993-1-4 (2015) has been taken into account to study the different failure mechanism of the column. Moreover the effect of curvature radius of cross-section and load capacity of the flat oval section for different length has been studied.

## 2. Finite element modelling

The finite element (FE) studies of flat oval thin class 4 section slender column under axial compression has been studied using the finite element software Abaqus. The typical cross section of flat oval column is shown in Fig. 1. The FE geometry, meshing and boundary condition of slender flat oval column are shown in Figs. 2(a), 2(b) and 2(c). Different curvature radius ($r$) of the curve portion has been considered keeping all other parameters constant. For LDSS material, constitutive material model proposed by Gardner and Ashraf (2006) (modified version of original Ramberg–Osgood (1943), Rasmussen (2003)) has been used. The shell finite elements (S4R) available in Abaqus were employed. The finite element modeling has been validated against experimental studies on square slender

*Corresponding author. Tel: +919957546722; E-mail address: 28sachi19@gmail.com

Proceedings of the 12th Structural Engineering Convention (SEC 2022), NCDMM, MNIT Jaipur, India| 19-22 December, 2022

Published online: December 19, 2022
doi:10.38208/acp.v1.675

LDSS hollow tubular columns reported by Theofanous and Gardner (2009). The same approached has been followed for further analysis in this study.

## 3. Geometry and boundary conditions

The geometry of flat oval section consists of two flat faces with rounded surfaces at both the ends. The nomenclature of the flat oval section has been considered as flat length ($l_f$), curvature radius ($r$), width between flat faces ($w$) and length ($h$) of column. The typical nomenclature of flat oval section has been named as $l50w50r25t2h2000$, which would represent $l_f = 50$ mm, $w = 50$ mm, $r = 25$ mm, $t = 2$ mm, $h = 2000$ mm respectively. For the boundary condition of the column, the bottom part is fixed while the axial compressive displacement was applied on the top through displacement control, with the top end being allowed to translate freely only in the axial direction. These boundary conditions were achieved through reference points RF1 and RF2, which are kinematically coupled (Abaqus). The geometries considered to find the effect of curvature radius varies in the range of 25 to 100 mm and the height of column varying from 1000 mm to 15000 mm. The column length has been varied in a wide range to capture the effect of different failure mechanism even if all the column comes under the slender column. The mesh size has been determined by the mesh convergence study ~ 8x8 mm with aspect ratio of ~1.

## 4. Geometric imperfections

The steel members are not free from imperfection mainly during the transportation and handling of equipments for lifting heavy metals. In modeling the real scenario of the steel has been considered. Following the reports in the literature, both the local and global mode shapes were scales with imperfection magnitudes of $t/100$ (see e.g. Theofanous *et al*., 2009, Chan and Gardner, 2008) and $h/1500$ (see e.g. Theofanous and Gardner, 2009, Patton and Singh, 2013) respectively.

## 5. Material modelling

The stress-strain curve of LDSS material has been derived, from the material properties given in Table 1 (Theofanous and Gardner, 2009), by following the material model pattern of Gardner and Ashraf (2006) (modified version of original Ramberg–Osgood (1943), Rasmussen (2003). Poisson's ratio was taken as 0.3. The stress (σ) - strain (ε) curve of LDSS material is shown in Fig. 3 consisting of two parts viz., (a) up to 0.2% proof stress (σ0.2), where Ramberg-Osgood model (1943) is used to define the curve, and (b) from σ0.2 to σ1.0, where Gardner and Ashraf model (2006) is used.

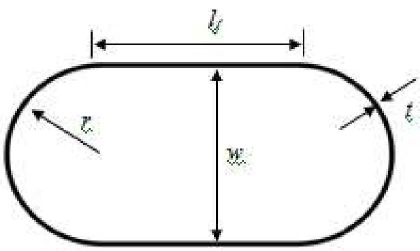


**Fig.1. Flat oval hollow section**

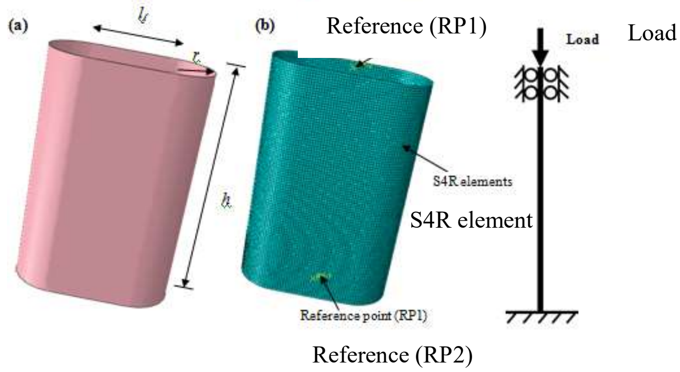


Fig. 2. Typical (a) FE geometry, (b) FE mesh and (c) boundary conditions of LDSS flat oval hollow column.

Table 1. Compressive flat material properties (Theofanous and Gardner, 2009).

| Cross-section | $E$ (MPa) | $\sigma_{0.2}$ (MPa) | $\sigma_{1.0}$ (MPa) | R-O coefficients | |
|---|---|---|---|---|---|
| | | | | $n$ | $n'_{0.2,1.0}$ |
| 80x80x4-SC2 | 197200 | 657 | 770 | 4.7 | 2.6 |

## 6. Verification of finite element model

The experimental investigation on slender SHC (square hollow column) conducted by Theofanous and Gardner (2009) are used to verify the developed FE modelling approach in term of load and lateral displacement at mid height of column. The material property in Fig. 3 is input in the ABAQUS model by converting into true stress ($\sigma_{true}$) and true plastic strain $\left(\varepsilon^{pl}_{true}\right)$ using the following Eqs.(1) and (2).

$$\sigma_{true} = \sigma_{nom}(1+\varepsilon_{nom}) \tag{1}$$

$$\varepsilon^{pl}{}_{true} = \ln(1+\varepsilon_{nom}) - \frac{\sigma_{true}}{E_o} \tag{2}$$

Where $\sigma_{nom}$ and $\varepsilon_{nom}$ are engineering stress and strain respectively

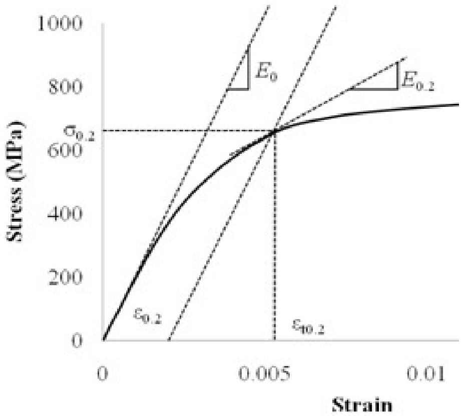


Fig. 3. Experimental stress-strain curve of LDSS material Grade EN 1.4162 (Theofanous & Gardner, 2009).

Table 2. Slender column dimensions (Theofanous and Gardner, 2009).

| Specimen | D (mm) | B (mm) | t (mm) | $r_i$ (mm) | Buckle length , $h_{cr}$ (mm) |
|---|---|---|---|---|---|
| 80x80x4-1200 | 79.3 | 79.6 | 3.72 | 3.8 | 1199.5 |
| 80x80x4-2000 | 79.6 | 79.5 | 3.80 | 3.4 | 1999.0 |

$h_{cr}$ = Buckling length, $D$ = Depth, $B$ = Width, $t$ = thickness, $r_i$ = internal corner radius

The geometric details of the validated experimental columns under axial compression are given in Table 2. The comparison of load-deformation curve of experimental and FE model of slender column (SHC 80x80x4-2000 and SHC 80x80x4-1200) (Theofanous and Gardner, 2009) are shown in Fig. 4. It can be seen that both the ultimate and post-ultimate curve profiles are well matched, thus indicating that the current FE modelling approach can provide reasonably accurate results for the modelling of LDSS hollow columns under axial compression.

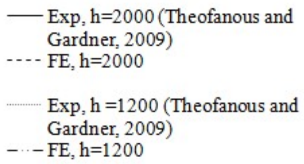


## 7. Parametric study

The parametric studies of flat oval slender columns were carried out by varying the curvature radius of the curve portion from 25 to 100 mm, height from 1000 mm to 15000 mm keeping all other parameters constant as $l_f$ = 50 mm, w = 50 mm and $t$ = 2 mm throughout the study. The entire analysis matrix results in Class 4 ($l_f/t\varepsilon$ > 37) following EN 1993-1-4 (2015). Based on the FE analyses, structural performance of the columns under axial compression were assessed, with attention towards, load capacity and deformation modes. Special observations are also made on the failure modes or mechanism both at ultimate (i.e. $\delta_u$) and post-ultimate (e.g. ~1.5 $\delta_u$) deformations.

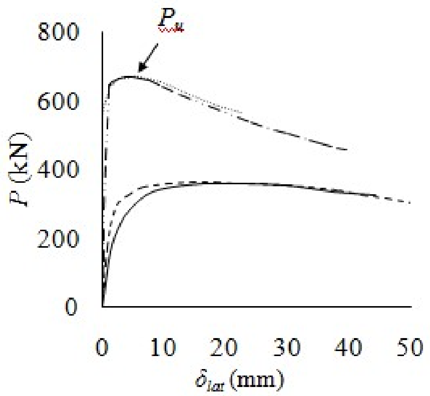


Fig. 4. Validation of $P$ (load) vs $\delta_{lat}$ (lateral displacement) for SHC 80x80x4 ($h$ =1200 mm and 2000 mm, (Theofanous & Gardner, 2009).

## 8. Results and discussions

The non-linear FE results of the flat oval LDSS hollow slender columns under axial compression have been presented in the form of different deformation or failure mechanism followed by the effect of curvature radius on the curve portion.

### *8.1. Deformation mechanisms*

Based on the FE analyses of flat oval hollow slender columns of slender sections (Class 4), three key failure or deformation mechanism have been identified, observing their deformation modes at $\delta_u$ (i.e. deformation corresponding to $P_u$) and 1.5 $\delta_u$, *viz.*, a) Local to local yielding (Mechanism SL1A), b) Local to local yielding flexural (Mechanism SL1B), and c) Flexural to flexural yielding (Mechanism SL2). The three deformation mechanisms are described below:

#### 8.1.1. Local to local yielded buckling (Mechanism SL1A)

The SL1A mechanism is generally classified based on the deformation mode of local buckling at $\delta_u$ and locally yielded buckling at post ultimate load (i.e. 1.5$\delta_u$). Fig. 5(a) showed the von-Mises contour plots superimposed on deformed shapes (at $\delta_u$ and 1.5 $\delta_u$) and Fig. 5(b) show the typical variation of normalised loads i.e. $P/P_y$ (where $P_y = Af_y$ is the gross yield load) with axial deformation / shortening ($\delta$). The results are presented for the specimen *l*50*w*50*r*75*t*2*h*1000. It can be seen from Fig. 5b that $P_u/P_y$ < 1.0 (although by a small margin). From Fig. 5a, it can be seen that at $P_u$ (or $\delta_u$), there is an initiation of local bucking in both the flat and curve elements for ~ 75% of the middle length (see inset Fig. E1 of Fig. 5). Also it can be observed that alternate buckled half wavelengths are also stressed to yield (shown by grey colour), while almost the rest of the specimens are highly stressed closed to yield, with the yielded area getting larger towards the mid length. This may be because, the value of $r$ (= 75 mm) is relatively larger, resulting in a flatter curve ($r$ = 25 mm would result in a semi-circular curve), with comparable dimensions with that of flat length ($l_f$ = 50 mm), and this coupled with a relatively less slender length (i.e. $h/l_f$ = 20), has possibly provided local buckling patterns on both the flat and curve elements. Further, because of the less slender length, flexural type of buckling is also prevented. As the deformation increases beyond $\delta_u$ (say 1.5 $\delta_u$), it is seen that the local buckling gets localised around the mid length, resulting in a significantly larger single local buckling (approaching localised crushing) at the mid-length (see inset Fig. E2 of Fig. 5). With this formation of a single localised buckling zone, the local buckling occurring elsewhere (i.e. away from the mid height) appears to have reduced their magnitudes with significant distressing due to redistribution of the stress to the weaker mid length zone. As a result, at 1.5 $\delta_u$, most region of the column are in elastic range, with the buckled middle zone (~ 12.5% length of the column length) stressing beyond the yield. From Fig. 5b, the closeness of $P_u/P_y$ value to 1.0, indicates that the column is able to resists nearly the gross section yield load at ultimate load. This may be related to the formation of a number of distributed local buckling on both the curve and flat elements for an extended length (~75% of the column length) at $P_u$, resulting in a higher load resistance, as evident from the alternate buckling half wavelength stressing beyond yield stress.

8.1.2. Local to local yielded flexural (Mechanism SL1B)

The plotting of von-Mises stress contour superimposed on deformed shape are shown in Fig. 6a, for the failure mechanism, Local to local yielded flexural (Mechanism SL1B). The typical variation of $P/P_y$ vs $\delta$ is shown in Fig. 6b. The plots in the Figs. 6 correspond to the specimen *l*75*w*50*r*25*t*2*h*2500. From Fig. 6a, it can be observed that, at $\delta_u$, occurrence of distributed local buckling can be seen on the flat elements, with stresses much below the yield stress, indicating elastic behaviour. The stress in the ~24% of the mid length portion appears to be slightly higher than the rest. This may be because, the length of the flat element is now relatively longer ($l_f$ = 75 mm) compared to the other cross-sectional dimensions, also the curve element is of semi-circular shape, which is known to have better buckling resistance than flat elements. At the post-$P_u$ i.e. at 1.5 $\delta_u$ a global or flexural type of deformation is seen along the weaker principle plane (see inset Fig. F2 of Fig. 6a). At three zones viz., around mid-length and at the two supports, yielding can be seen, characteristic of flexural bending of fixed ended column. The size of the yielded zones are about ~12% and ~6% of the column length for the mid-length and end zones respectively, although at the support ends, the formation of the yielded zone is towards the compression sides (at least at 1.5 $\delta_u$). At 1.5 $\delta_u$, it can also be seen that local buckling is not totally eliminated (as in the Mechanism SL1A), although they (with possibly reduced lateral deflection magnitudes) are mostly visible around the mid length portion (~50% of the column length). From Fig. 6b, it is observed that the occurrence of flexural buckling has significantly reduced the load capacity, as indicated by a lower value of $P_u/P_y$ (~0.5).

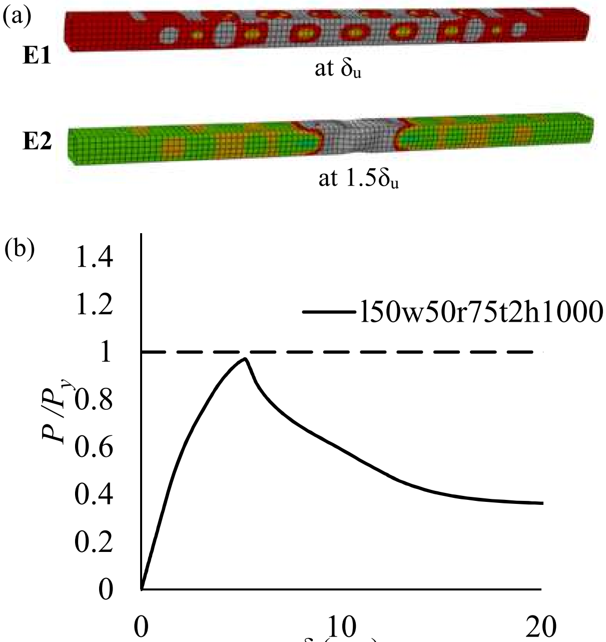


Fig. 5. Typical Mechanism SL1A (local to local buckling) failure mode: a) von-Misses contour plot of E1 (at $\delta_u$) and E2 (at 1.5$\delta_u$); b) variation of $P/P_y$ with $\delta$ for (*l*50*w*50*r*75*t*2*h*1000).

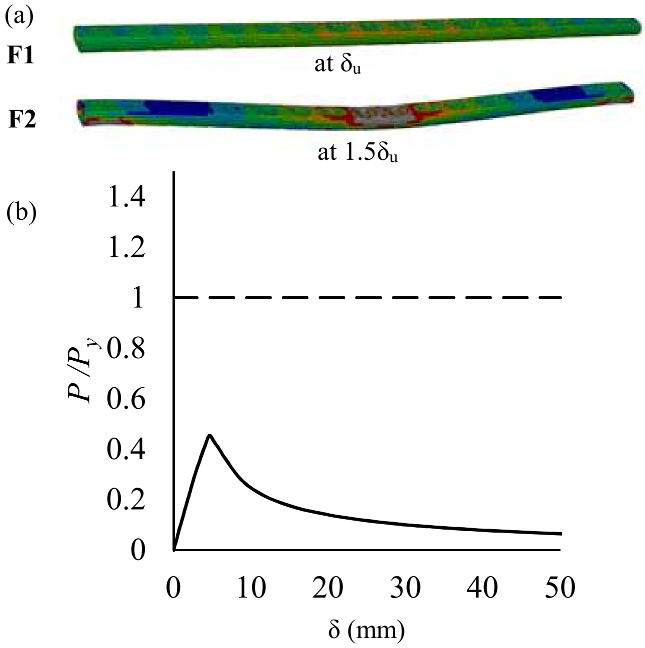


Fig. 6. Typical Mechanism SL1B (local to local-flexural buckling) failure mode: a) von-Misses contour plot of F1 (at $\delta_u$) and F2 (at 1.5$\delta_u$); b) variation of $P/P_{cr}$ with δ (axial aaaadeformation), and c) variation of $P/P_y$ with $\delta$ (*l*75*w*50*r*25*t*2*h*2500).

8.1.3. Flexural to flexural yielding (Mechanism SL2)

The plot of von-mises stress contour superimposed on deformed shapes (corresponding to $\delta_u$ and 1.5$\delta_u$), for the specimen *l*50*w*50*r*50*t*2*h*3500, depicting the flexural to flexural yielding (Mechanism SL2) mechanism has been shown in Fig. 7a and the typical $P/P_y$ with $\delta$ has been shown in Fig. 7b. At $\delta_u$, the column has shown signs of initiation of flexural buckling with a relatively uniform higher stress around a major portion in the mid-length together with a much reduced stress at the ends (see inset G1 in Fig. 7a). At 1.5 $\delta_u$, a distinct flexural deformation mode is seen with yielded zone being formed at mid-length, and supports ends, for ~25% and 7% of the column length respectively. It is interesting to note that, for this particular example, the axis of flexural bending is perpendicular to the flat element, and hence the yielding is mostly seen on the curve surface. This kind of behaviour may have been influenced by the imperfection mode shape seeded in FE. From Fig. 7b, it is observed that $P_u/P_y$ = 0.4. The $P_u/P_y$ is much lower than 1, suggesting that the overall failure mechanism is flexural or elastic.

*8.2. Effect of curvature radius (r)*

The variation of ultimate load ($P_u$) capacity of column along with the changes in curvature radius ($r$) of cross-section for different length of column is shown in Fig. 8. Fig. 8 showed that the $P_u$ of column is the maximum at the semi-circular ($r/w$ = 0.5 at $r$ = 25 mm) curve section as compared to the flatter curve section i.e., $P_u$ showed negligible changes for flatter curve section ($r/w$ > 0.5). $P_u$ of column reduces as the length of column increases (i.e., higher slenderness ratio, $\lambda = h_e$(effective length)/$K$(Radius of gyration)) and its rate of reduction reduces in very long slender columns and the maximum reduction happens in case of intermediate column

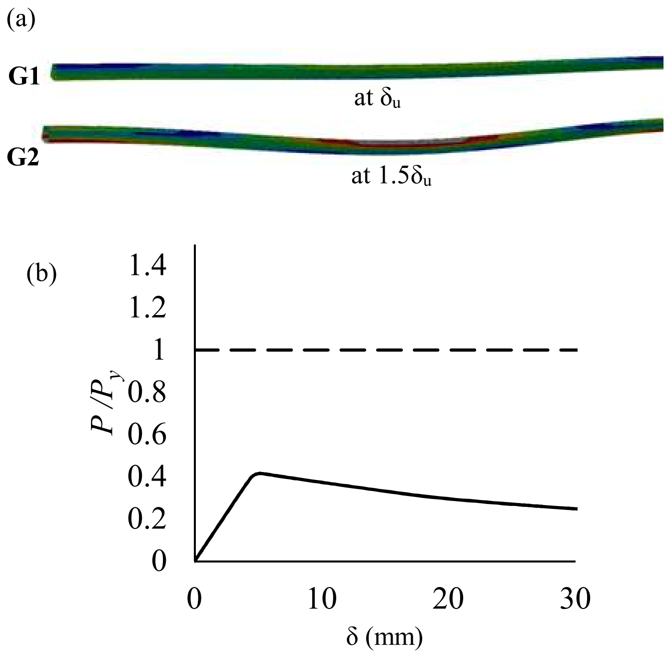


Fig. 7. Typical Mechanism SL2 (flexural to flexural buckling) failure mode: a) von-Misses contour plot of G1 (at $\delta_u$) and G2 (at $1.5\delta_u$); b) variation of $P/P_y$ with δ ($l50w50r50t2h3500$).

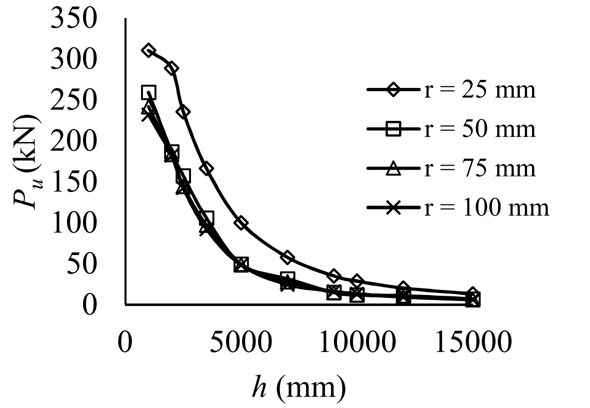


**Fig. 8. Comparison of $P_u$ vs $h$ at $t$ = 2 mm, $h$ = 1000-15000 mm, $l_f$ = 50 mm, $w$ = 50 mm, $r$ = 25-100 mm**

ranges ~3500 to 9000 mm. As the slenderness length of column increases, there is no significant effect of the cross-section showing minimal difference in ultimate load of column

## 9. Conclusions

Based on the parametric study of flat oval column, the following conclusions have been derived as follows.

1) The failure mechanism of flat oval thin slender column can be observed with various interactive buckling pattern from local to local yielded, local to local yielded flexure, flexure to flexure mechanism as the loading changes from pre to post ultimate loading according to the increase in the slenderness of the cross-section.
2) It is observed that buckling mechanism determined the failure pattern of the column.
3) The $P_u$ of column decreases with increase in slenderness ratio. The decrease rate of $P_u$ is maximum at intermediate column but longer column, there is slight decrease in the $P_u$ of column.
4) $P_u$ is the highest for $r/w$ = 0.5 (flat oval with semi-circle curve face) and decreases as the curvature becomes flatter.

## References

1. ABAQUS.(2009). Abaqus/Standard ., *Dassault Systems Corporation*, USA.
2. Chan, T.M., & Gardner, L. (2008). Compressive resistance of hot-rolled elliptical hollow sections. *Engineering Structures*, 30(2), 522-32.
3. EN 10088-4(2009). Stainless steels part 4: Technical delivery conditions for sheet/plate and strip of corrosion resisting steels for general purposes. CEN 2009.
4. EN 1993-1-4 (2015). Eurocode 3 – Design of steel structures – Part 1-4:. General rules – Supplementary rules for stainless steel. EN 1993-1-4: 2006+A1:CEN.
5. Ellobody, E., & Young, B. (2007). Investigation of cold-formed stainless steel non slender circular hollow section columns. *Steel and Composite Structures,* 7(4), 321-337.
6. Gardner,L., & Ministro, A. (2004). Testing and numerical modelling of structural steel oval hollow sections. *Department of civil and environmental engineering, Imperial college, London, 04-002-ST* .
7. Gardner,L. & Ashraf, M. (2006). Structural design for non-linear metallic materials. *Engineering Structures,* 28, 925-36.
8. Liu,Y., & Young, B. (2003). Buckling of stainless steel square hollow section compression members*. Journal of Constructional Steel Research*, 59, 165-77.
9. Patton, M.L., & Singh, K.D., (2012). Numerical modeling of lean duplex stainless steel hollow columns of square, L-,T-,and +-shaped cross sections under pure axial compression. *Thin-Walled Structures*, 53, 1-8.
10. Patton, M.L., & Singh, K.D. (2013). Buckling of Fixed-Ended Lean Duplex Stainless Steel Hollow Columns of Square, L-, T-, and +-Shaped Sections under Pure Axial Compression—a Finite Element Study. *Thin-Walled Structures*, 63, 106-16.
11. Rasmussen, K.J.R., (2003). Full-range stress-strain curves for stainless steel alloys. *Journal of Constructional Steel Research*, 59, 47-61.
12. Ramberg, W., & Osgood, W.R. (1943). Description of stress-strain curves by three parameters. *Technical Note No 902*, Washington, DC: *National advisory committee for aeronautics*.
13. Theofanous, M. & Gardner,L. (2010). Experimental and numerical studies of lean duplex stainless steel beams. *Journal of Constructional Steel Research,* 66(6), 816-825.
14. Theofanous, M., & Gardner, L., (2009). Testing and numerical modelling of lean duplex stainless steel hollow section columns. *Engineering Structures*, 31, 3047-58.
15. Theofanous, M., Chan, T.M . & Gardner, L.(2009). Structural response of stainless steel oval hollow section under compression members. *Engineering Structures*, 31, 922-934.
16. Zhu,J., & Young, B. (2011). Cold-formed-steel oval hollow sections under axial compression. *Journal of Structural Engineering*, 137(7) (2011) 719-727.
17. Zhu, J., & Young, B. (2012). Design of cold-formed steel oval hollow section columns. *Journal of Constructional Steel Research*, 71, 26-37.